Nonlinear Dyn (2022) 110:3605–3615
https://doi.org/10.1007/s11071-022-07767-y

ORIGINAL PAPER

On multi-soliton solutions to a generalized inhomogeneous nonlinear Schrödinger equation for the Heisenberg ferromagnetic spin chain

Zhou-Zheng Kang · Rong-Cao Yang

Received: 9 May 2022 / Accepted: 28 July 2022 / Published online: 23 August 2022

Abstract A generalized inhomogeneous higher-order nonlinear Schrödinger (GIHNLS) equation for the Heisenberg ferromagnetic spin chain system in (1+1)-dimensions under zero boundary condition at infinity is taken into account. The spectral analysis is first performed to generate a related matrix Riemann–Hilbert problem on the real axis. Then, through solving the resulting matrix Riemann–Hilbert problem by taking the jump matrix to be the identity matrix, the general bright multi-soliton solutions to the GIHNLS equation are attained. Furthermore, the one-, two-, and three-soliton solutions are written out and analyzed by figures.

Keywords Higher-order nonlinear Schrödinger equation · Riemann–Hilbert problem · Soliton solutions

1 Introduction

Solitons are stable, nonlinear pulses which show a fine balance between nonlinearity and dispersion. They often arise from some real physical phenomena described by integrable nonlinear partial differential equations (NLPDEs) modeling shallow water waves, nonlinear optics, electrical network pulses and many other applications in mathematical physics [1–3]. Both theoretical and experimental investigations [4–6] have been made on solitons. The derivation of abundant soliton solutions [7,8] to NLPDEs has been closely concerned by scholars from mathematics and physics, and a variety of approaches and their extentions have been established and applicable to NLPDEs up to present, such as the Hirota's bilinear method [9,10], the Darboux transformation [11,12], the Riemann–Hilbert method [13–15], and the Lie symmetry method [16, 17]. In the past years, a considerable literature has grown up around the applications of the Riemann–Hilbert technique to solve integrable NLPDEs with zero or nonzero boundary condition, some of which include the coupled NLS equation [18], the Kundu–Eckhaus equation [19], the six-component fourth-order AKNS system [20], the multicomponent mKdV system [21], the N-coupled Hirota equation [22], and the fifth-order NLS equation [23].

In this paper, we focus on a generalized inhomogeneous higher-order nonlinear Schrödinger (GIHNLS) equation for the Heisenberg ferromagnetic spin system [26] in (1+1)-dimensions

$$\begin{aligned} &iu_t + \epsilon u_{xxxx} + 8\epsilon |u|^2 u_{xx} + 2\epsilon u^2 u^*_{xx} \\ &\quad +4\epsilon u_x u^*_x u + 6\epsilon u^* u_x^2 + 6\epsilon |u|^4 u \\ &\quad + \left(\frac{1}{2} - 3\epsilon\right) u_{xx} + (1-6\epsilon) u^2 u^* - ihu_x = 0, \end{aligned} \tag{1}$$

where u denotes the complex function of the scaled spatial variable x and temporal variable t, the real number ϵ is a perturbation parameter, the real number h stands

Z.-Z. Kang (✉)· R.-C. Yang
School of Physics and Electronic Engineering, Shanxi University, Taiyuan 030006, China
e-mail: zhzhkang@126.com

for the inhomogeneities in the medium [24,25], and the asterisk and subscripts mean the complex conjugation and partial derivatives, respectively. Equation (1) is an integrable model. When $h = 0$, Eq. (1) reduces to the fourth-order NLS equation, which governs the Davydov solitons in the alpha helical protein with higher-order effects [27]. In the past, many studies have been conducted on Eq. (1). The Lax pair [24] was first presented. The gauge transformation was used to construct soliton solutions [26]. The generalized Darboux technique was applied to generate some higher-order rogue wave solutions [28]. In a follow-up study, some solutions were computed by Hirota's bilinear method, and infinitely many conservation laws were derived based upon the AKNS system [29].

The rest of the paper is arranged as follows. In Sect. 2, we formulate a matrix Riemann–Hilbert problem by carrying out the spectral analysis and obtain the reconstruction formula of potential. In Sect. 3, we gain soliton solutions from a specific Riemann–Hilbert problem on the real axis, in which the jump matrix is taken as the identity matrix. The final section is a brief conclusion.

2 Matrix Riemann–Hilbert problem

What we intend to describe in this section is a matrix Riemann–Hilbert problem. We start by considering the Lax pair [28] for Eq. (1)

$$\phi_x = U\phi, \tag{2}$$
$$\phi_t = V\phi, \tag{3}$$

where $\phi = (\phi_1, \phi_2)^{\mathrm{T}}$ is the spectral function, the symbol T stands for the vector transpose, and $\lambda \in \mathbb{C}$ is a spectral parameter. And

$$U = \begin{pmatrix} -i\lambda & u \\ -u^* & i\lambda \end{pmatrix}, \quad V = \begin{pmatrix} V_{11} & V_{12} \\ -V_{21} & -V_{11} \end{pmatrix},$$
$$\begin{aligned}
V_{11} &= 2\epsilon\lambda u_x u^* - i\epsilon u_x u_x^* + i\epsilon u_{xx} u^* - 4i\epsilon\lambda^2 uu^* \\
&\quad -2\epsilon\lambda uu_x^* + 3i\epsilon u^2 (u^*)^2 - 3i\epsilon uu^* + i\epsilon uu_{xx}^* \\
&\quad +\frac{1}{2} iuu^* - ih\lambda - i\lambda^2 + 8i\epsilon\lambda^4 + 6i\epsilon\lambda^2, \\
V_{12} &= 6i\epsilon uu_x u^* + 4\epsilon\lambda u^2 u^* + hu - 4i\epsilon\lambda^2 u_x + 2\epsilon\lambda u_{xx} \\
&\quad -3i\epsilon u_x + i\epsilon u_{xxx} + \frac{1}{2} iu_x + \lambda u - 8\epsilon\lambda^3 u - 6\epsilon\lambda u, \\
V_{21} &= hu^* + \lambda u^* - 8\epsilon\lambda^3 u^* + 4i\epsilon\lambda^2 u_x^* \\
&\quad +4\epsilon\lambda u(u^*)^2 - 6\epsilon\lambda u^* + 2\epsilon\lambda u_{xx}^* + 3i\epsilon u_x^* \\
&\quad -6i\epsilon uu^* u_x^* - i\epsilon u_{xxx}^* - \frac{1}{2} iu_x^*.
\end{aligned}$$

Equivalently, the Lax pair (2) and (3) reads

$$\phi_x = (-i\lambda\Lambda + Q)\phi, \tag{4}$$
$$\phi_t = \big((8i\epsilon\lambda^4 + 6i\epsilon\lambda^2 - i\lambda^2 - ih\lambda)\Lambda + V_1\big)\phi, \tag{5}$$

in which $\Lambda = \mathrm{diag}(1, -1)$ and

$$Q = \begin{pmatrix} 0 & u \\ -u^* & 0 \end{pmatrix}, \quad V_1 = \begin{pmatrix} \tilde{V}_{11} & \tilde{V}_{12} \\ -\tilde{V}_{21} & -\tilde{V}_{11} \end{pmatrix},$$
$$\begin{aligned}
\tilde{V}_{11} &= 2\epsilon\lambda u_x u^* - i\epsilon u_x u_x^* + i\epsilon u_{xx} u^* \\
&\quad -4i\epsilon\lambda^2 uu^* - 2\epsilon\lambda uu_x^* + 3i\epsilon u^2 (u^*)^2 \\
&\quad -3i\epsilon uu^* + i\epsilon uu_{xx}^* + \frac{1}{2} iuu^* \\
\tilde{V}_{12} &= 6i\epsilon uu_x u^* + 4\epsilon\lambda u^2 u^* + hu - 4i\epsilon\lambda^2 u_x \\
&\quad +2\epsilon\lambda u_{xx} - 3i\epsilon u_x + i\epsilon u_{xxx} \\
&\quad +\frac{1}{2} iu_x + \lambda u - 8\epsilon\lambda^3 u - 6\epsilon\lambda u, \\
\tilde{V}_{21} &= hu^* + \lambda u^* - 8\epsilon\lambda^3 u^* \\
&\quad +4i\epsilon\lambda^2 u_x^* + 4\epsilon\lambda u(u^*)^2 - 6\epsilon\lambda u^* \\
&\quad +2\epsilon\lambda u_{xx}^* + 3i\epsilon u_x^* - 6i\epsilon uu^* u_x^* \\
&\quad -i\epsilon u_{xxx}^* - \frac{1}{2} iu_x^*.
\end{aligned}$$

In our analysis, we suppose the potential u to be vanished rapidly at infinity. It is evident to see from (4) and (5) that $\phi \sim e^{-i\lambda\Lambda x + (8i\epsilon\lambda^4 + 6i\epsilon\lambda^2 - i\lambda^2 - ih\lambda)\Lambda t}$. Thus, we introduce the transformation

$$\phi = \psi e^{-i\lambda\Lambda x + (8i\epsilon\lambda^4 + 6i\epsilon\lambda^2 - i\lambda^2 - ih\lambda)\Lambda t},$$

which enable us to convert the Lax pair (4) and (5) into

$$\psi_x = -i\lambda[\Lambda, \psi] + Q\psi, \tag{6}$$
$$\psi_t = (8i\epsilon\lambda^4 + 6i\epsilon\lambda^2 - i\lambda^2 - ih\lambda)[\Lambda, \psi] + V_1\psi, \tag{7}$$

where the square brackets denote the usual matrix commutator, namely $[\Lambda, \psi] = \Lambda\psi - \psi\Lambda$.

In what follows, the spectral problem (6) will be analyzed, and t will be treated as a constant. We represent the matrix Jost solutions $\psi_\pm(x, \lambda)$ as

$$\psi_\pm(x, \lambda) = ([\psi_\pm]_1, [\psi_\pm]_2)(x, \lambda), \tag{8}$$

with the boundary conditions

$$\psi_\pm(x, \lambda) \to \mathbf{I}_2, \quad x \to \pm\infty. \tag{9}$$

The above subscripts in ψ refer to which end of the x-axis the boundary conditions are required for, and

$\mathbf{I}_2$ is the identity matrix of size 2. Using the boundary conditions (9), one obtains Volterra-type integral equations

$$\psi_-(x,\lambda) = \mathbf{I}_2 + \int_{-\infty}^{x} e^{-i\lambda\Lambda(x-z)} Q(z)\psi_-(z,\lambda)e^{i\lambda\Lambda(x-z)}\mathrm{d}z, \tag{10}$$

$$\psi_+(x,\lambda) = \mathbf{I}_2 - \int_{x}^{+\infty} e^{-i\lambda\Lambda(x-z)} Q(z)\psi_+(z,\lambda)e^{i\lambda\Lambda(x-z)}\mathrm{d}z. \tag{11}$$

From (10) and (11), we find that $[\psi_+]_1$ and $[\psi_-]_2$ are analytic for $\lambda \in \mathbb{C}_-$ and continuous for $\lambda \in \mathbb{C}_- \cup \mathbb{R}$, while $[\psi_-]_1$ and $[\psi_+]_2$ are analytic for $\lambda \in \mathbb{C}_+$ and continuous for $\lambda \in \mathbb{C}_+ \cup \mathbb{R}$, where $\mathbb{C}_-$ and $\mathbb{C}_+$ are the lower and upper half λ-plane. Applying the Abel's identity, we reveal that $\det \psi_\pm$ are independent of x, since $\mathrm{tr}Q = 0$. Evaluating $\det \psi_-$ at $x = -\infty$ and $\det \psi_+$ at $x = +\infty$, we have $\det \psi_\pm = 1$ for $\forall x$ and $\lambda \in \mathbb{R}$. Due to matrix solutions of (4), $\psi_- e^{-i\lambda\Lambda x}$ and $\psi_+ e^{-i\lambda\Lambda x}$ are linearly associated by the scattering matrix $S(\lambda)$

$$\psi_- e^{-i\lambda\Lambda x} = \psi_+ e^{-i\lambda\Lambda x} S(\lambda), \quad S(\lambda) = \begin{pmatrix} s_{11} & s_{12} \\ s_{21} & s_{22} \end{pmatrix}, \quad \lambda \in \mathbb{R}. \tag{12}$$

We notice that $\det S(\lambda) = 1$ due to $\det \psi_\pm(x,\lambda) = 1$.

A matrix Riemann–Hilbert problem is associated with two matrix analytic functions. In view of the analytic properties of $\psi_\pm$, the analytic function in $\mathbb{C}_+$ is given by

$$P_1(x,\lambda) = ([\psi_-]_1, [\psi_+]_2)(x,\lambda) = \psi_- A_1 + \psi_+ A_2, \tag{13}$$

in which

$$A_1 = \mathrm{diag}(1,0), \quad A_2 = \mathrm{diag}(0,1). \tag{14}$$

Because P_1 solves (6), we make an asymptotic expansion for P_1 at large-λ

$$P_1 = P_1^{(0)} + \frac{P_1^{(1)}}{\lambda} + \frac{P_1^{(2)}}{\lambda^2} + O\left(\frac{1}{\lambda^3}\right), \quad \lambda \to \infty,$$

and substitute the asymptotic expansion into (6). Comparing the coefficients of the same powers of λ yields

$$O(1): P_{1x}^{(0)} = -i\left[\Lambda, P_1^{(1)}\right] + QP_1^{(0)};$$

$$O(\lambda): -i\left[\Lambda, P_1^{(0)}\right] = 0.$$

Thus, we see that $P_1^{(0)} = \mathbf{I}_2$, namely $P_1 \to \mathbf{I}_2$ as $\lambda \in \mathbb{C}_+ \to \infty$.

For construction of a matrix Riemann–Hilbert problem, we still need the analytic counterpart of P_2 in $\mathbb{C}_-$. Consider the adjoint equation of (6)

$$\kappa_x = -i\lambda[\Lambda, \kappa] - \kappa Q. \tag{15}$$

One can verify that the inverse matrices

$$\psi_\pm^{-1}(x,\lambda) = \begin{pmatrix} [\psi_\pm^{-1}]^1 \\ [\psi_\pm^{-1}]^2 \end{pmatrix}(x,\lambda) \tag{16}$$

solve (15). Here, $[\psi_\pm^{-1}]^j (j = 1,2)$ signify the j-th row of $\psi_\pm^{-1}$ and follow the boundary conditions $\psi_\pm^{-1}(x,\lambda) \to \mathbf{I}_2$ as $x \to \pm\infty$. From (12), it follows immediately that

$$\psi_-^{-1} = e^{-i\lambda\Lambda x} S^{-1}(\lambda) e^{i\lambda\Lambda x} \psi_+^{-1}, \quad \lambda \in \mathbb{R}, \tag{17}$$

where $S^{-1}(\lambda) = (r_{lk})_{2\times 2}$. Thus, the analytic function P_2 in $\mathbb{C}_-$ is expressed as

$$P_2(x,\lambda) = \begin{pmatrix} [\psi_-^{-1}]^1 \\ [\psi_+^{-1}]^2 \end{pmatrix}(x,\lambda) = A_1\psi_-^{-1} + A_2\psi_+^{-1}, \tag{18}$$

where A_1 and A_2 are given by (14). One can find that the asymptotic behavior of P_2 turns out to be $P_2 \to \mathbf{I}_2$ as $\lambda \to \infty$.

Inserting $\psi_\pm(x,\lambda)$ into (12) gives

$$[\psi_-]_1 = s_{11}[\psi_+]_1 + s_{21}e^{2i\lambda x}[\psi_+]_2.$$

The $\psi_\pm^{-1}(x,\lambda)$ are then substituted into (17) yielding

$$[\psi_-^{-1}]^1 = r_{11}[\psi_+^{-1}]^1 + r_{12}e^{-2i\lambda x}[\psi_+^{-1}]^2.$$

Thus, P_1 and P_2 can be represented as

$$P_1 = ([\psi_-]_1, [\psi_+]_2) = ([\psi_+]_1, [\psi_+]_2)\begin{pmatrix} s_{11} & 0 \\ s_{21}e^{2i\lambda x} & 1 \end{pmatrix},$$

$$P_2 = \begin{pmatrix} [\psi_-^{-1}]^1 \\ [\psi_+^{-1}]^2 \end{pmatrix} = \begin{pmatrix} r_{11} & r_{12}e^{-2i\lambda x} \\ 0 & 1 \end{pmatrix}\begin{pmatrix} [\psi_+^{-1}]^1 \\ [\psi_+^{-1}]^2 \end{pmatrix}.$$

Having presented two matrix functions P_1 and P_2 which are analytic in $\mathbb{C}_+$ and $\mathbb{C}_-$, respectively, a matrix Riemann–Hilbert problem on the real axis can be formed below

$$P^-(x,\lambda)P^+(x,\lambda) = G(x,\lambda) = \begin{pmatrix} 1 & r_{12}e^{-2i\lambda x} \\ s_{21}e^{2i\lambda x} & 1 \end{pmatrix}, \quad \lambda \in \mathbb{R}, \tag{19}$$

in which we have denoted that $P_1 \to P^+$ as $\lambda \in \mathbb{C}_+ \to \mathbb{R}$ and $P_2 \to P^-$ as $\lambda \in \mathbb{C}_- \to \mathbb{R}$. And the canonical normalization conditions are given by

$$P_1(x,\lambda) \to \mathbf{I}_2, \quad \lambda \in \mathbb{C}_+ \to \infty; \quad P_2(x,\lambda) \to \mathbf{I}_2, \quad \lambda \in \mathbb{C}_- \to \infty.$$

Next, we are going to present the reconstruction formula of the potential. Since $P_1(x,\lambda)$ solves (6), expanding $P_1(x,\lambda)$ at large-λ as

$$P_1 = \mathbf{I}_2 + \frac{P_1^{(1)}}{\lambda} + \frac{P_1^{(2)}}{\lambda^2} + O\left(\frac{1}{\lambda^3}\right), \quad \lambda \to \infty,$$

and inserting this expansion into (6), we see that

$$Q = i\left[\Lambda, P_1^{(1)}\right] = \begin{pmatrix} 0 & 2i\left(P_1^{(1)}\right)_{12} \\ -2i\left(P_1^{(1)}\right)_{21} & 0 \end{pmatrix} \Longrightarrow u = 2i\left(P_1^{(1)}\right)_{12},$$

where $\left(P_1^{(1)}\right)_{12}$ is the (1,2)-entry of $P_1^{(1)}$. By now, we have achieved the reconstruction for the potential.

3 Soliton solutions

For calculation of soliton solutions to Eq. (1), we make an assumption that det $P_1(\lambda)$ and det $P_2(\lambda)$ can be zeros at certain discrete locations in analytic domains. Based on det $\psi_\pm = 1$, (13) and (18), as well as the scattering relation (12), we reveal that det $P_1(\lambda) = s_{11}(\lambda)$ and det $P_2(\lambda) = r_{11}(\lambda)$. That is to say, det $P_1(\lambda)$ and det $P_2(\lambda)$ have the same zeros as $s_{11}(\lambda)$ and $r_{11}(\lambda)$. We now need the locations of zeros. Notice that the potential matrix Q satisfies the anti-Hermitian property $Q^\dagger = -Q$, where $\dagger$ means the matrix Hermitian. Taking advantage of this property in Q, one has

$$\psi_\pm^\dagger(x,\lambda^*) = \psi_\pm^{-1}(x,\lambda). \tag{20}$$

After taking the Hermitian to (13) and considering (18), we find that

$$P_1^\dagger(\lambda^*) = P_2(\lambda), \quad \lambda \in \mathbb{C}_-, \tag{21}$$

and

$$S^\dagger(\lambda^*) = S^{-1}(\lambda) \Longrightarrow s_{11}^*(\lambda^*) = r_{11}(\lambda).$$

From this, it is found that each zero λ_j of det P_1 produces each zero λ_j^* of det P_2. Let N be a free natural number. Generally, we assume that det P_1 and det P_2 have some simple zeros at $\lambda_j \in \mathbb{C}_+$ and $\hat{\lambda}_j = \lambda_j^* \in \mathbb{C}_-$, respectively. For this case, each of the kernel of $P_1(\lambda_j)$ and $P_2(\hat{\lambda}_j)$ contains a single basis column vector v_j or row vector $\hat{v}_j$:

$$P_1(\lambda_j)v_j = 0, \tag{22}$$

$$\hat{v}_j P_2(\hat{\lambda}_j) = 0, \tag{23}$$

By taking the Hermitian to (22) and utilizing (21), we get

$$\hat{v}_j = v_j^\dagger, \quad 1 \le j \le N. \tag{24}$$

Then, computing x-derivative and t-derivative in (22), respectively, and using (6) and (7) yields

$$P_1(\lambda_j)\left(\frac{\partial v_j}{\partial x} + i\lambda_j \Lambda v_j\right) = 0,$$

$$P_1(\lambda_j)\left(\frac{\partial v_j}{\partial t} - (8i\epsilon\lambda_j^4 + 6i\epsilon\lambda_j^2 - i\lambda_j^2 - ih\lambda_j)\Lambda v_j\right) = 0.$$

Therefore, we get

$$v_j = e^{\left(-i\lambda_j x + (8i\epsilon\lambda_j^4 + 6i\epsilon\lambda_j^2 - i\lambda_j^2 - ih\lambda_j)t\right)\Lambda} v_{j0}.$$

In view of the relation (24), we see that

$$\hat{v}_j = v_{j0}^\dagger e^{\left(i\lambda_j^* x - (8i\epsilon\lambda_j^{*4} + 6i\epsilon\lambda_j^{*2} - i\lambda_j^{*2} - ih\lambda_j^*)t\right)\Lambda},$$

where v_{j0} and $v_{j0}^\dagger$ are constants.

For presenting soliton solutions, we consider the reflectionless case, namely $G(x,\lambda) = \mathbf{I}_2$. This resulting special Riemann–Hilbert problem [30] possesses the solutions

$$P_1(\lambda) = \mathbf{I}_2 - \sum_{k=1}^{N}\sum_{j=1}^{N} \frac{v_k \hat{v}_j \left(M^{-1}\right)_{kj}}{\lambda - \hat{\lambda}_j},$$

$$P_2(\lambda) = \mathbf{I}_2 + \sum_{k=1}^{N}\sum_{j=1}^{N} \frac{v_k \hat{v}_j \left(M^{-1}\right)_{kj}}{\lambda - \lambda_k}, \tag{25}$$

where $M = (m_{kj})_{N\times N}$ and

$$m_{kj} = \frac{\hat{v}_k v_j}{\lambda_j - \hat{\lambda}_k}, \quad 1 \le k, j \le N.$$

From Eq. (25), we derive

$$P_1^{(1)} = -\sum_{k=1}^{N}\sum_{j=1}^{N} v_k \hat{v}_j \left(M^{-1}\right)_{kj}.$$

Combining the established results with $\nu_{j0} = (a_j, b_j)^{\mathrm{T}}$ and $\vartheta_j = -i\lambda_j x + (8i\epsilon\lambda_j^4 + 6i\epsilon\lambda_j^2 - i\lambda_j^2 - ih\lambda_j)t$, the general N-soliton solution to Eq. (1) can be written as

$$u(x,t) = -2i\sum_{k=1}^{N}\sum_{j=1}^{N} a_k b_j^* e^{\vartheta_k - \vartheta_j^*}\left(M^{-1}\right)_{kj},$$

$$m_{kj} = \frac{1}{\lambda_j - \lambda_k^*}\left(a_k^* a_j e^{\vartheta_k^* + \vartheta_j} + b_k^* b_j e^{-\vartheta_k^* - \vartheta_j}\right).$$

In what follows, we intend to discuss one-, two-, and three-soliton solutions graphically.

(i) For $N = 1$, Eq. (1) possesses one-soliton solution

$$u(x,t) = \frac{4a_1 b_1^* \lambda_{12} e^{\vartheta_1 - \vartheta_1^*}}{|a_1|^2 e^{\vartheta_1^* + \vartheta_1} + |b_1|^2 e^{-\vartheta_1^* - \vartheta_1}}, \tag{26}$$

where we have assumed $\vartheta_1 = -i\lambda_1 x + (8i\epsilon\lambda_1^4 + 6i\epsilon\lambda_1^2 - i\lambda_1^2 - ih\lambda_1)t$ and $\lambda_1 = \lambda_{11} + i\lambda_{12}$. Further, upon assuming $b_1 = 1$ and $|a_1|^2 = e^{2\xi_1}$, then the solution (26) can be written as

$$u(x,t) = 2a_1\lambda_{12}e^{-\xi_1}e^{\vartheta_1 - \vartheta_1^*}\operatorname{sech}(\vartheta_1^* + \vartheta_1 + \xi_1), \tag{27}$$

where $\vartheta_1^* + \vartheta_1 = 2\lambda_{12}x + (64\epsilon\lambda_{11}\lambda_{12}^3 - 64\epsilon\lambda_{11}^3\lambda_{12} - 24\epsilon\lambda_{11}\lambda_{12} + 2h\lambda_{12} + 4\lambda_{11}\lambda_{12})t$ and $\vartheta_1 - \vartheta_1^* = -2i\lambda_{11}x - 2i(-8\epsilon\lambda_{11}^4 + (48\epsilon\lambda_{12}^2 - 6\epsilon + 1)\lambda_{11}^2 + h\lambda_{11} + (-8\lambda_{12}^4 + 6\lambda_{12}^2)\epsilon - \lambda_{12}^2)t$. Equivalently, the solution (27) reads

$$\begin{aligned} u(x,t) = 2a_1\lambda_{12}e^{-\xi_1}e^{\vartheta_1 - \vartheta_1^*}\operatorname{sech}\big[&2\lambda_{12}x + \big(64\epsilon\lambda_{11}\lambda_{12}^3 \\ &-64\epsilon\lambda_{11}^3\lambda_{12} - 24\epsilon\lambda_{11}\lambda_{12} \\ &+2h\lambda_{12} + 4\lambda_{11}\lambda_{12}\big)t + \xi_1\big]. \end{aligned} \tag{28}$$

According to expression (28), we know that the amplitude function $|u(x,t)|$ has a sech profile. This soliton with peak amplitude $2|a_1|\lambda_{12}e^{-\xi_1}$ travels at velocity $-32\epsilon\lambda_{11}\lambda_{12}^2 + 32\epsilon\lambda_{11}^3 + 12\epsilon\lambda_{11} - h - 2\lambda_{11}$ depending on both real and imaginary parts of the spectral parameter λ_1, unlike the basic NLS equation. The phase relies on the spatial variable x and temporal variable t linearly. The soliton in Fig. 1 is formed for $a_1 = 1, \lambda_1 = \frac{1}{6} + \frac{i}{2}, \xi_1 = 0, \epsilon = 1, h = 1$. From Fig. 1b, it is seen that the wave travels from right to left along the x-axis over time.

(ii) For $N = 2$, two-soliton solution is given by

$$u(x,t) = -\frac{2i\left(a_1 b_1^* m_{22} e^{\vartheta_1 - \vartheta_1^*} - a_1 b_2^* m_{12} e^{\vartheta_1 - \vartheta_2^*} - a_2 b_1^* m_{21} e^{\vartheta_2 - \vartheta_1^*} + a_2 b_2^* m_{11} e^{\vartheta_2 - \vartheta_2^*}\right)}{m_{11}m_{22} - m_{12}m_{21}}, \tag{29}$$

where

$$\begin{aligned} m_{11} &= \frac{1}{\lambda_1 - \lambda_1^*}\left(|a_1|^2 e^{\vartheta_1^* + \vartheta_1} + |b_1|^2 e^{-\vartheta_1^* - \vartheta_1}\right), \\ m_{12} &= \frac{1}{\lambda_2 - \lambda_1^*}\left(a_1^* a_2 e^{\vartheta_1^* + \vartheta_2} + b_1^* b_2 e^{-\vartheta_1^* - \vartheta_2}\right), \\ m_{21} &= \frac{1}{\lambda_1 - \lambda_2^*}\left(a_2^* a_1 e^{\vartheta_2^* + \vartheta_1} + b_2^* b_1 e^{-\vartheta_2^* - \vartheta_1}\right), \\ m_{22} &= \frac{1}{\lambda_2 - \lambda_2^*}\left(|a_2|^2 e^{\vartheta_2^* + \vartheta_2} + |b_2|^2 e^{-\vartheta_2^* - \vartheta_2}\right), \end{aligned}$$

and $\vartheta_\iota = -i\lambda_\iota x + (8i\epsilon\lambda_\iota^4 + 6i\epsilon\lambda_\iota^2 - i\lambda_\iota^2 - ih\lambda_\iota)t$, $\lambda_\iota = \lambda_{\iota 1} + i\lambda_{\iota 2}$, $\iota = 1, 2$. Through assuming $a_1 = a_2$, $b_1 = b_2 = 1$, and $|a_1|^2 = e^{2\xi_1}$, the solution (29) reads

$$u(x,t) = -\frac{2i\left(a_1 m_{22} e^{\vartheta_1 - \vartheta_1^*} - a_1 m_{12} e^{\vartheta_1 - \vartheta_2^*} - a_2 m_{21} e^{\vartheta_2 - \vartheta_1^*} + a_2 m_{11} e^{\vartheta_2 - \vartheta_2^*}\right)}{m_{11}m_{22} - m_{12}m_{21}}, \tag{30}$$

in which

$$\begin{aligned} m_{11} &= -\frac{ie^{\xi_1}}{\lambda_{12}}\cosh(\vartheta_1^* + \vartheta_1 + \xi_1), \\ m_{12} &= \frac{2e^{\xi_1}}{(\lambda_{21} - \lambda_{11}) + i(\lambda_{12} + \lambda_{22})}\cosh(\vartheta_1^* + \vartheta_2 + \xi_1), \\ m_{22} &= -\frac{ie^{\xi_1}}{\lambda_{22}}\cosh(\vartheta_2^* + \vartheta_2 + \xi_1), \\ m_{21} &= \frac{2e^{\xi_1}}{(\lambda_{11} - \lambda_{21}) + i(\lambda_{12} + \lambda_{22})}\cosh(\vartheta_2^* + \vartheta_1 + \xi_1). \end{aligned}$$

In order to show interaction behaviors between two solitons, some graphs are plotted and two cases are under consideration here.

We first consider the case of two solitons traveling at different velocities. In this case, the solution parameters in (30) are first chosen as $a_1 = 1, a_2 = 1, \lambda_1 = \frac{1}{10} + \frac{i}{3}, \lambda_2 = \frac{1}{10} + \frac{i}{2}, \xi_1 = 0, \epsilon = 1, h = 1$. According

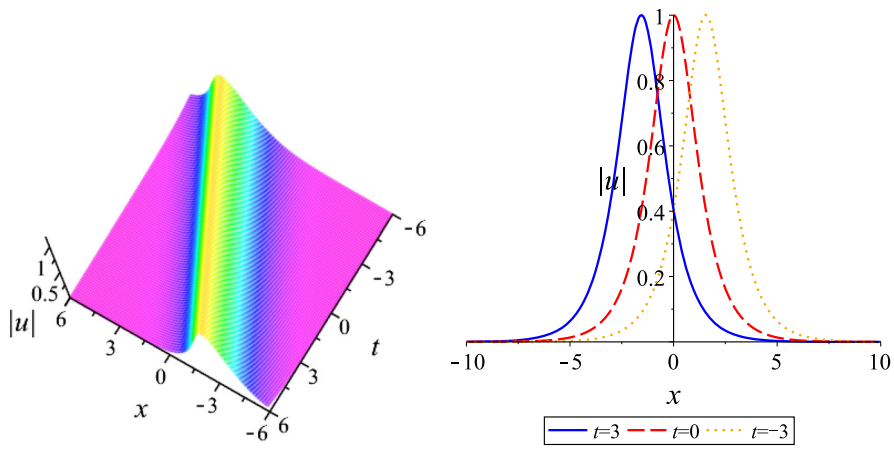

(a) **(b)**

Fig. 1 Profiles of one-soliton solution (28) with $a_1 = 1, \lambda_1 = \frac{1}{6} + \frac{i}{2}, \xi_1 = 0, \epsilon = 1, h = 1$. **a** 3D plot; **b** x-curves

to these values, some plots are made to shed light on the localization and dynamical behaviors. Figure 2a shows the localized structure of this solution on (x, t)-plane clearly, which is a typical cross two bright solitons. It can be observed that the overtaking collision between the solitons takes place as depicted in Fig. 2b, where two solitons with different velocities move together toward the same direction along the x-axis. The (taller) soliton with a larger amplitude travels much faster than the other (shorter) soliton with a smaller amplitude, and the taller soliton catches up with the shorter soliton over time. Both solitons then continue to proceed in the same direction. At the moment $t = 0$, the amplitude value for two solitons reaches the maximum. Before and after the collision, their speeds and shapes are unchanged. In other words, the overtaking is an elastic interaction.

In Fig. 3, we show the head-on collision between two solitons with the parameters as $a_1 = 1, a_2 = 1, \lambda_1 = \frac{1}{10} + \frac{i}{2}, \lambda_2 = \frac{1}{6} + \frac{i}{3}, \xi_1 = 0, \epsilon = 1, h = 1$. The taller soliton crashes the shorter one in the opposite direction of the x-axis. After the collision, their amplitudes, widths, speeds, and directions are same as those before only except phase shifts, see Fig. 3b. Evidently, the head-on interaction of two solitons is also elastic.

With regard to the second case, we consider that two solitons travel at same speeds. The solution parameters in (30) are specified as $a_1 = 1, a_2 = 1, \lambda_1 = \frac{i}{3}, \lambda_2 = \frac{i}{2}, \xi_1 = 0, \epsilon = 1, h = 1$. The bound state of two solitons is shown on (x, t)-plane in Fig. 4, in which two solitons are localized spatially and keep together in propagation. Indeed, this solution indicates the breather, namely when two solitons propagate, the amplitude function is periodic in oscillation over time.

(iii) For $N = 3$, Eq. (1) admits three-soliton solution

$$\begin{aligned} u(x,t) = -\frac{2i}{\varrho}\big[&a_1 b_1^*(m_{22}m_{33} - m_{23}m_{32})e^{\vartheta_1-\vartheta_1^*} \\ &- a_1 b_2^*(m_{12}m_{33} - m_{13}m_{32})e^{\vartheta_1-\vartheta_2^*} \\ &+ a_1 b_3^*(m_{12}m_{23} - m_{13}m_{22})e^{\vartheta_1-\vartheta_3^*} \\ &- a_2 b_1^*(m_{21}m_{33} - m_{23}m_{31})e^{\vartheta_2-\vartheta_1^*} \\ &+ a_2 b_2^*(m_{11}m_{33} - m_{13}m_{31})e^{\vartheta_2-\vartheta_2^*} \\ &- a_2 b_3^*(m_{11}m_{23} - m_{13}m_{21})e^{\vartheta_2-\vartheta_3^*} \\ &+ a_3 b_1^*(m_{21}m_{32} - m_{22}m_{31})e^{\vartheta_3-\vartheta_1^*} \\ &- a_3 b_2^*(m_{11}m_{32} - m_{12}m_{31})e^{\vartheta_3-\vartheta_2^*} \\ &+ a_3 b_3^*(m_{11}m_{22} - m_{12}m_{21})e^{\vartheta_3-\vartheta_3^*}\big], \end{aligned} \tag{31}$$

where $\varrho = m_{11}m_{22}m_{33} - m_{11}m_{23}m_{32} - m_{12}m_{21}m_{33} + m_{12}m_{23}m_{31} + m_{13}m_{21}m_{32} - m_{13}m_{22}m_{31}$,

$$m_{11} = \frac{1}{\lambda_1 - \lambda_1^*}\left(|a_1|^2 e^{\vartheta_1^*+\vartheta_1} + |b_1|^2 e^{-\vartheta_1^*-\vartheta_1}\right),$$

$$m_{12} = \frac{1}{\lambda_2 - \lambda_1^*}\left(a_1^* a_2 e^{\vartheta_1^*+\vartheta_2} + b_1^* b_2 e^{-\vartheta_1^*-\vartheta_2}\right),$$

$$m_{13} = \frac{1}{\lambda_3 - \lambda_1^*}\left(a_1^* a_3 e^{\vartheta_1^*+\vartheta_3} + b_1^* b_3 e^{-\vartheta_1^*-\vartheta_3}\right),$$

$$m_{21} = \frac{1}{\lambda_1 - \lambda_2^*}\left(a_2^* a_1 e^{\vartheta_2^*+\vartheta_1} + b_2^* b_1 e^{-\vartheta_2^*-\vartheta_1}\right),$$

$$m_{22} = \frac{1}{\lambda_2 - \lambda_2^*}\left(|a_2|^2 e^{\vartheta_2^*+\vartheta_2} + |b_2|^2 e^{-\vartheta_2^*-\vartheta_2}\right),$$

$$m_{23} = \frac{1}{\lambda_3 - \lambda_2^*}\left(a_2^* a_3 e^{\vartheta_2^*+\vartheta_3} + b_2^* b_3 e^{-\vartheta_2^*-\vartheta_3}\right),$$

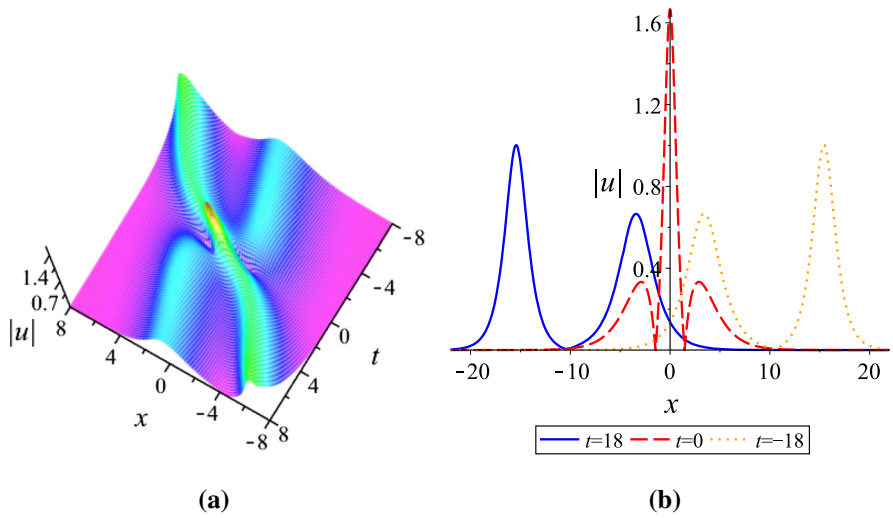

(a) **(b)**

Fig. 2 Profiles of two-soliton solution (30) with $a_1 = 1, a_2 = 1, \lambda_1 = \frac{1}{10} + \frac{i}{3}, \lambda_2 = \frac{1}{10} + \frac{i}{2}, \xi_1 = 0, \epsilon = 1, h = 1$. **a** 3D plot; **b** x-curves

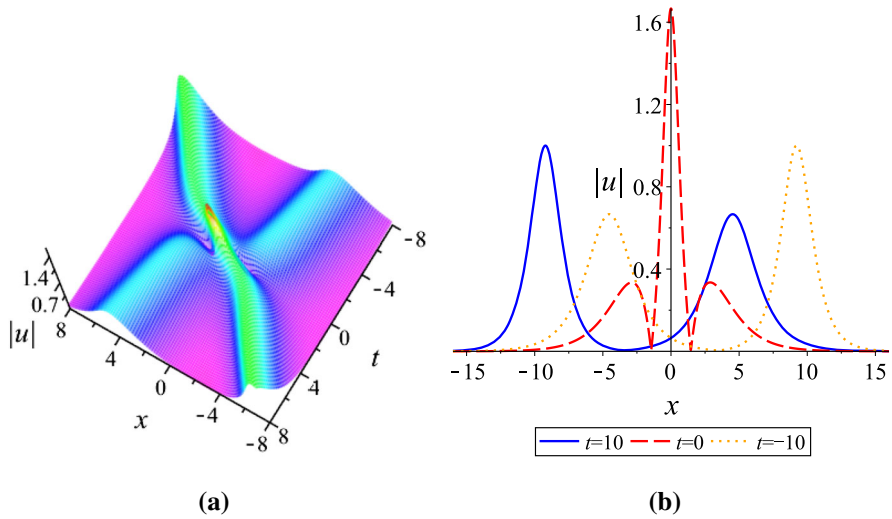

(a) **(b)**

Fig. 3 Profiles of two-soliton solution (30) with $a_1 = 1, a_2 = 1, \lambda_1 = \frac{1}{10} + \frac{i}{2}, \lambda_2 = \frac{1}{6} + \frac{i}{3}, \xi_1 = 0, \epsilon = 1, h = 1$. **a** 3D plot; **b** x-curves

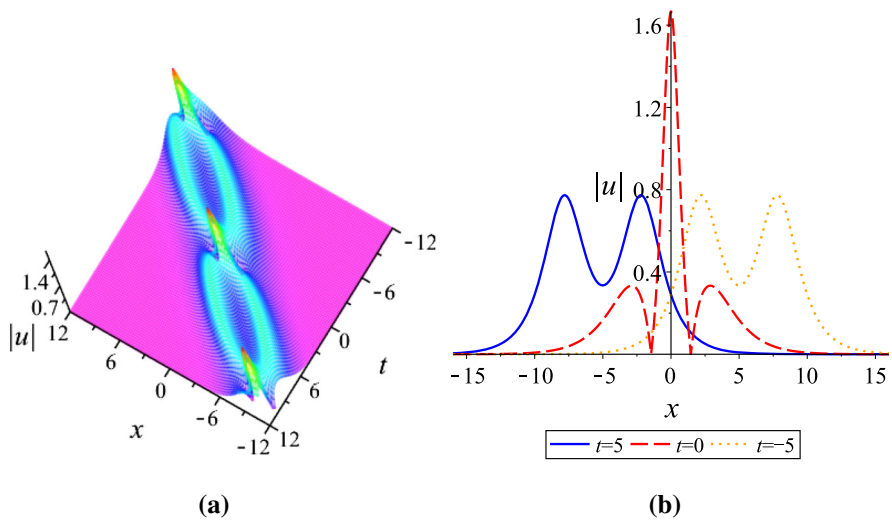

(a) **(b)**

Fig. 4 Profiles of two-soliton solution (30) with $a_1 = 1, a_2 = 1, \lambda_1 = \frac{i}{3}, \lambda_2 = \frac{i}{2}, \xi_1 = 0, \epsilon = 1, h = 1$. **a** 3D plot; **b** x-curves

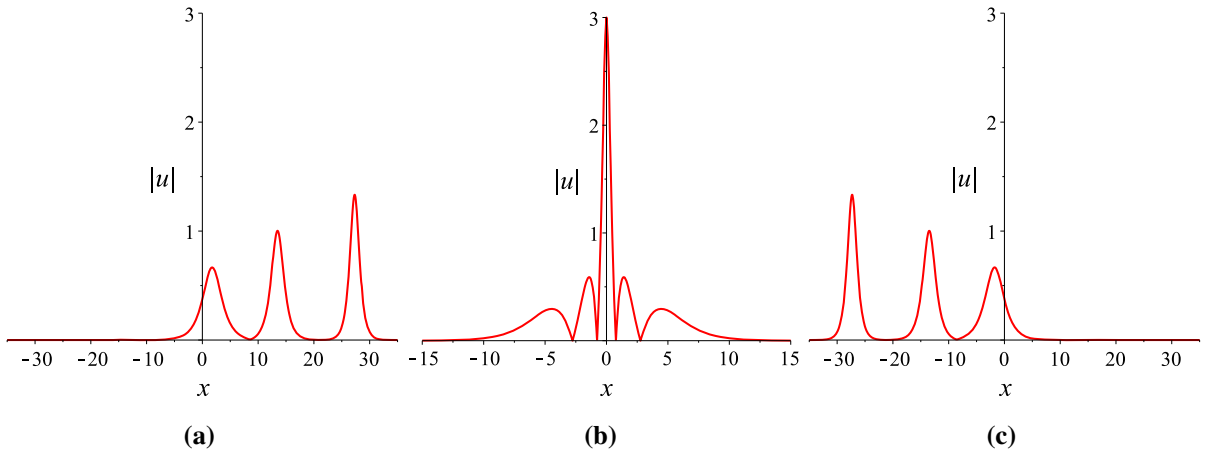

Fig. 5 Profiles of three-soliton solution (31) with $a_1 = 1, a_2 = 1, a_3 = 1, b_1 = 1, b_2 = 1, b_3 = 1, \lambda_1 = \frac{1}{10} + \frac{i}{2}, \lambda_2 = \frac{1}{10} + \frac{2i}{3}, \lambda_3 = \frac{1}{10} + \frac{i}{3}, \epsilon = 1, h = 1$. **a** x-curve at $t = -18$; **b** x-curve at $t = 0$; **c** x-curve at $t = 18$

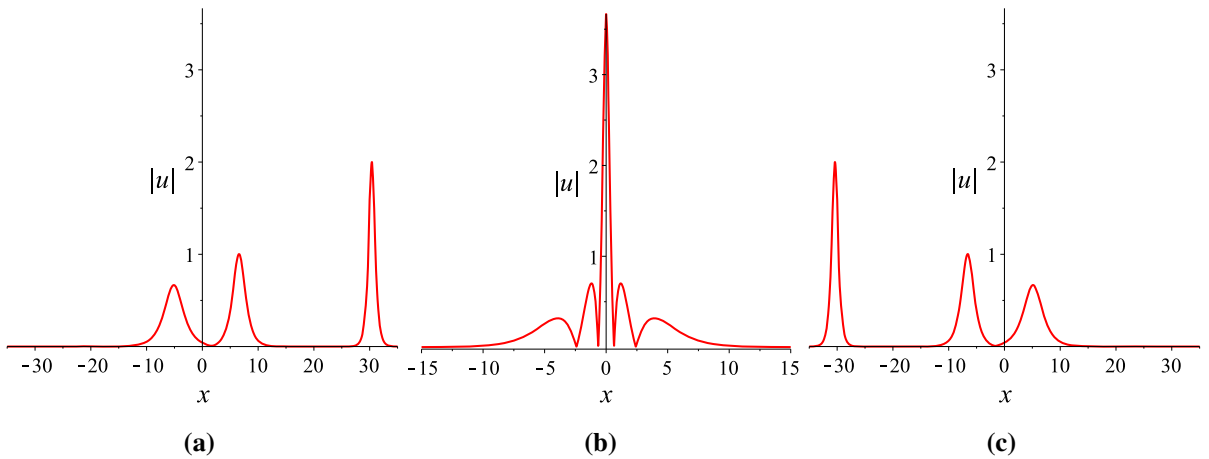

Fig. 6 Profiles of three-soliton solution (31) with $a_1 = 1, a_2 = 1, a_3 = 1, b_1 = 1, b_2 = 1, b_3 = 1, \lambda_1 = \frac{1}{10} + \frac{i}{2}, \lambda_2 = \frac{1}{6} + \frac{i}{3}, \lambda_3 = \frac{1}{8} + i, \epsilon = 1, h = 1$. **a** x-curve at $t = -8$; **b** x-curve at $t = 0$; **c** x-curve at $t = 8$

$$m_{31} = \frac{1}{\lambda_1 - \lambda_3^*}\left(a_3^* a_1 e^{\vartheta_3^* + \vartheta_1} + b_3^* b_1 e^{-\vartheta_3^* - \vartheta_1}\right),$$
$$m_{32} = \frac{1}{\lambda_2 - \lambda_3^*}\left(a_3^* a_2 e^{\vartheta_3^* + \vartheta_2} + b_3^* b_2 e^{-\vartheta_3^* - \vartheta_2}\right),$$
$$m_{33} = \frac{1}{\lambda_3 - \lambda_3^*}\left(|a_3|^2 e^{\vartheta_3^* + \vartheta_3} + |b_3|^2 e^{-\vartheta_3^* - \vartheta_3}\right),$$

and $\vartheta_\iota = -i\lambda_\iota x + (8i\epsilon\lambda_\iota^4 + 6i\epsilon\lambda_\iota^2 - i\lambda_\iota^2 - ih\lambda_\iota)t$, $\lambda_\iota = \lambda_{\iota 1} + i\lambda_{\iota 2}$, $\iota = 1, 2, 3$.

Following the similar lines as our discussion on two solitons, we now examine the dynamics among three solitons. The parameter values in (31) are first given by $a_1 = 1, a_2 = 1, a_3 = 1, b_1 = 1, b_2 = 1, b_3 = 1, \lambda_1 = \frac{1}{10} + \frac{i}{2}, \lambda_2 = \frac{1}{10} + \frac{2i}{3}, \lambda_3 = \frac{1}{10} + \frac{i}{3}, \epsilon = 1, h = 1$. Based on these values, a special solution can be gained at once. And we can know the velocity relation for the three solitons $S_1 < S_2 < S_3$. Here, we have denoted that the solitons from left to right in Fig. 5a are S_1, S_2, and S_3. Figure 5 presents an elastic overtaking process among three solitons moving together toward the negative direction of the x-axis. Ultimately as time evolves, S_2 overtakes S_1, and S_3 overtakes S_1 and S_2. When $t = 0$, the peak amplitude is maximum.

Then, we take the parameters as $a_1 = 1, a_2 = 1, a_3 = 1, b_1 = 1, b_2 = 1, b_3 = 1, \lambda_1 = \frac{1}{10} + \frac{i}{2}, \lambda_2 = \frac{1}{6} + \frac{i}{3}, \lambda_3 = \frac{1}{8} + i, \epsilon = 1, h = 1$. Denoting that the solitons from left to right in Fig. 6a are s_1, s_2, and s_3,

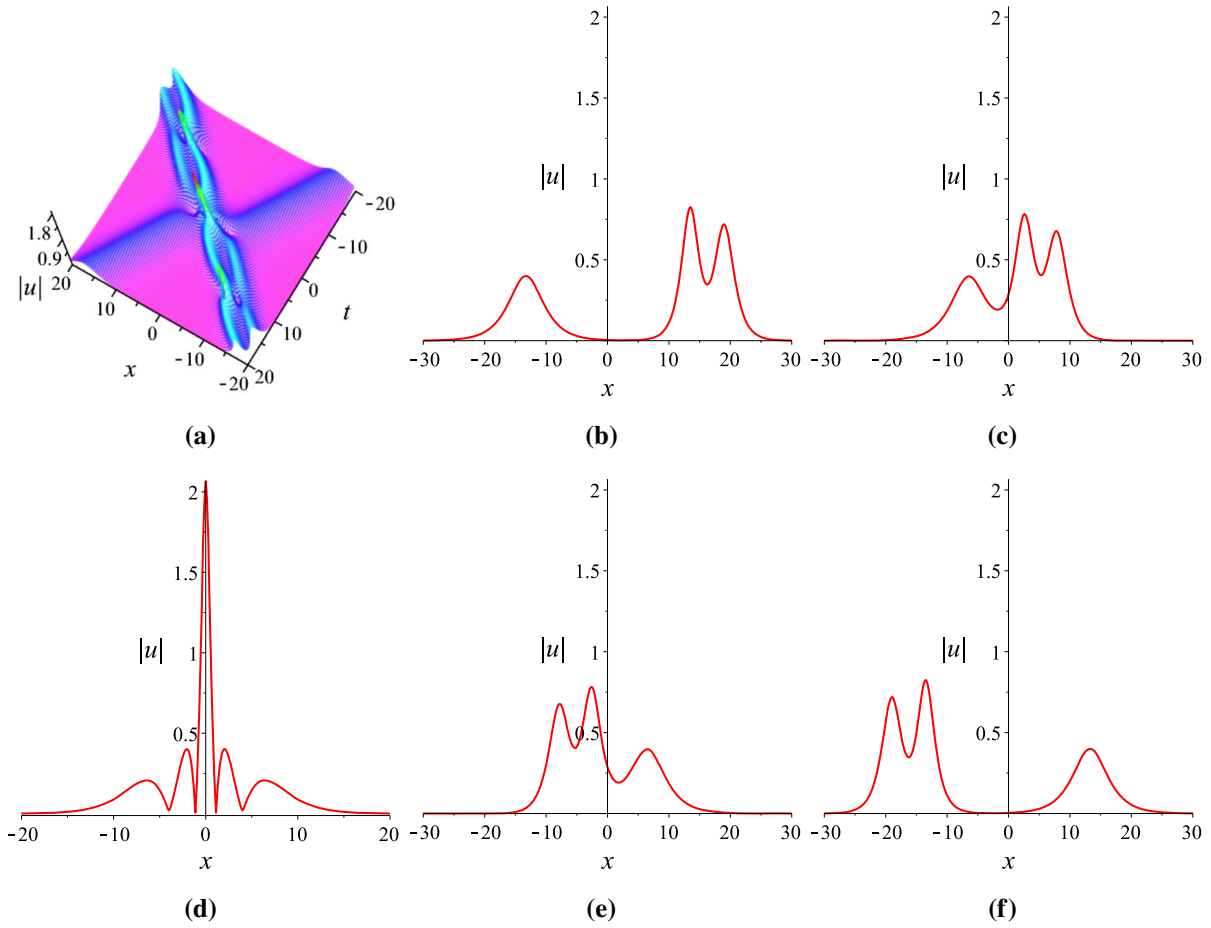

Fig. 7 Profiles of three-soliton solution (31) with $a_1 = 1, a_2 = 1, a_3 = 1, b_1 = 1, b_2 = 1, b_3 = 1, \lambda_1 = \frac{i}{2}, \lambda_2 = \frac{1}{6} + \frac{i}{5}, \lambda_3 = \frac{i}{3}, \epsilon = 1, h = 1$. **a** 3D plot; **b** x-curve at $t = -15$; **c** x-curve at $t = -\frac{15}{4}$; **d** x-curve at $t = 0$; **e** x-curve at $t = \frac{15}{4}$; **f** x-curve at $t = 15$

respectively, it is found in Fig. 6 that s_1 moves toward the positive direction of the x-axis, which is opposite to the propagation direction of s_2 and s_3. As time goes on, s_1 collides head-on with s_2 and s_3, while s_3 overtakes s_2. After the interactions, the three solitons s_1, s_2, and s_3 continue to move along their original directions. Both head-on and overtaking interactions in the process are elastic. Additionally, the head-on interaction of two solitons in bound state with another soliton during propagation can be observed in Fig. 7. And Fig. 8 shows the evolution of bound state of three solitons.

4 Conclusion

In this study, a generalized inhomogeneous higher-order nonlinear Schrödinger equation for the Heisenberg ferromagnetic spin chain system in (1+1) -dimensions with the zero boundary condition was taken into account. A matrix Riemann–Hilbert problem was built, based on which multi-bright-soliton solutions to the examined equation were explored eventually. Moreover, the explicit forms of one-, two-, and three-bright-soliton solutions were given, and a few vivid plots were made to exhibit their spatial struc-

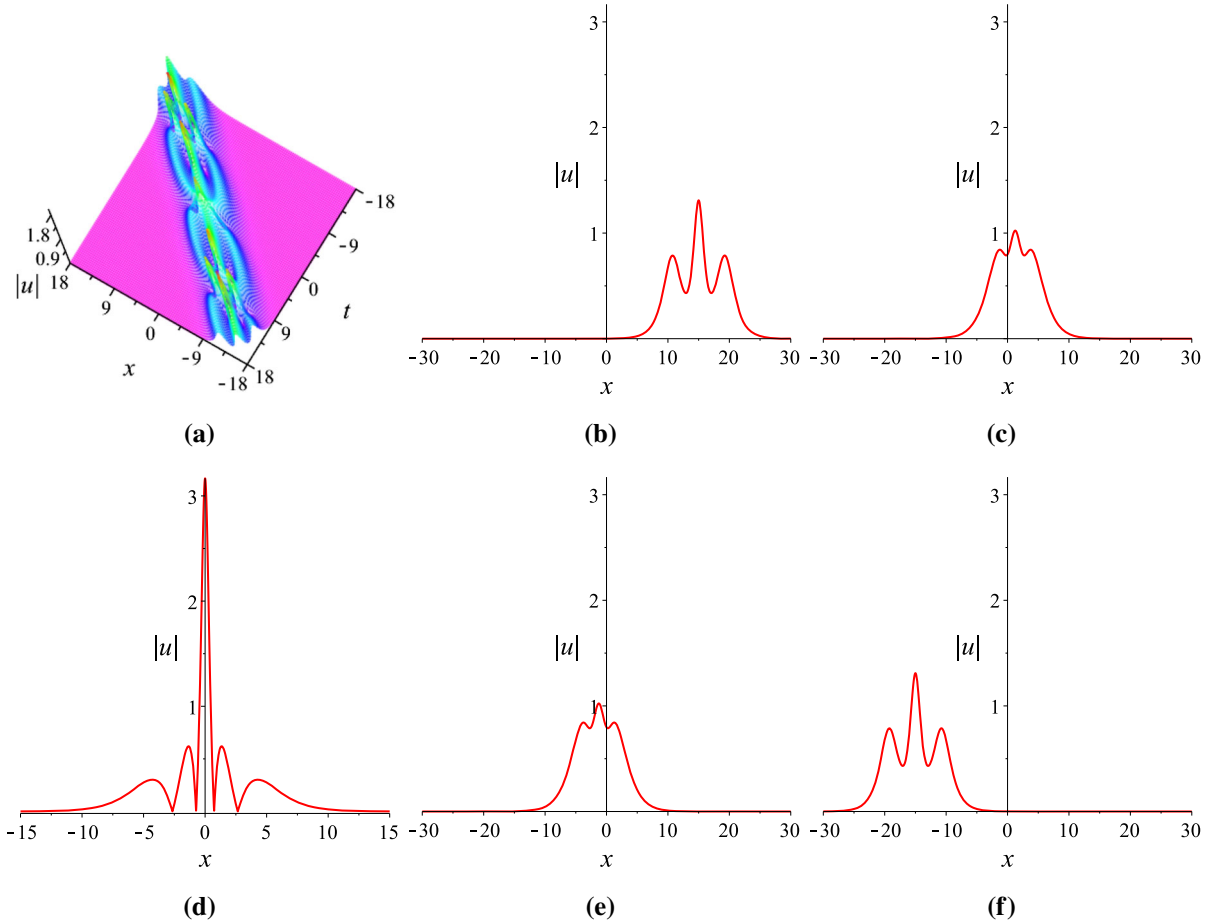

Fig. 8 Profiles of three-soliton solution (31) with $a_1 = 1, a_2 = 1, a_3 = 1, b_1 = 1, b_2 = 1, b_3 = 1, \lambda_1 = \frac{i}{2}, \lambda_2 = \frac{i}{3}, \lambda_3 = \frac{3i}{4}, \epsilon = 1, h = 1$. **a** 3D plot; **b** x-curve at $t = -15$; **c** x-curve at $t = -\frac{5}{4}$; **d** x-curve at $t = 0$; **e** x-curve at $t = \frac{5}{4}$; **f** x-curve at $t = 15$

tures in three-dimensions and dynamical behaviors in two-dimensions after specifying the parameter values properly with the aid of Maple software.

Funding This work is supported by the National Natural Science Foundation of China (Grant No. 61775126).

Data availability Our manuscript has no associated data.

Declarations

Conflict of interest The authors declare that they have no conflict of interest.

References

1. Enns, R.H., Jones, B.L., Miura, R.M., Rangnekar, S.S.: Nonlinear phenomena in physics and biology. Springer, New York (1981)
2. Griffiths, G.W., Schiesser, W.E.: Linear and nonlinear waves. Scholarpedia **4**, 4308 (2009)
3. Wen, X.K., Feng, R., Lin, J.H., Liu, W., Chen, F., Yang, Q.: Distorted light bullet in a tapered graded-index waveguide with PT symmetric potentials. Optik **248**, 168092 (2021)
4. Cao, Q.H., Dai, C.Q.: Symmetric and anti-symmetric solitons of the fractional second- and third-order nonlinear Schrödinger equation. Chin. Phys. Lett. **38**, 090501 (2021)
5. Wang, R.R., Wang, Y.Y., Dai, C.Q.: Influence of higher-order nonlinear effects on optical solitons of the complex Swift–Hohenberg model in the mode-locked fiber laser. Opt. Laser Tech. **152**, 108103 (2022)

6. Fang, J.J., Mou, D.S., Zhang, H.C., Wang, Y.Y.: Discrete fractional soliton dynamics of the fractional Ablowitz–Ladik model. Optik **228**, 166186 (2021)
7. Dai, C.Q., Wang, Y.Y.: Coupled spatial periodic waves and solitons in the photovoltaic photorefractive crystals. Nonlinear Dyn. **102**, 1733–1741 (2020)
8. Chen, Y.X.: Combined optical soliton solutions of a (1+1)-dimensional time fractional resonant cubic-quintic nonlinear Schrödinger equation in weakly nonlocal nonlinear media. Optik **203**, 163898 (2020)
9. Wazwaz, A.M., El-Tantawy, S.A.: Solving the (3+1)-dimensional KP-Boussinesq and BKP-Boussinesq equations by the simplified Hirota's method. Nonlinear Dyn. **88**, 3017–3021 (2017)
10. Zhang, S., Tian, C., Qian, W.Y.: Bilinearization and new multisoliton solutions for the (4+1)-dimensional Fokas equation. Pramana **86**, 1259–1267 (2016)
11. Yu, F.J., Feng, L.L., Li, L.: Darboux transformation for super-Schrödinger equation, super-Dirac equation and their exact solutions. Nonlinear Dyn. **88**, 1257–1271 (2017)
12. Xu, T., Chen, Y.: Mixed interactions of localized waves in the three-component coupled derivative nonlinear Schrödinger equations. Nonlinear Dyn. **92**, 2133–2142 (2018)
13. Ma, W.X.: Riemann–Hilbert problems and N-soliton solutions for a coupled mKdV system. J. Geom. Phys. **132**, 45–54 (2018)
14. Wu, J.P.: Riemann–Hilbert approach of the Newell-type long-wave-short-wave equation via the temporal-part spectral analysis. Nonlinear Dyn. **98**, 749–760 (2019)
15. Wu, J.P.: Integrability aspects and multi-soliton solutions of a new coupled Gerdjikov–Ivanov derivative nonlinear Schrödinger equation. Nonlinear Dyn. **96**, 789–800 (2019)
16. Kumar, S., Kumar, A.: Lie symmetry reductions and group invariant solutions of (2+1)-dimensional modified Veronese web equation. Nonlinear Dyn. **98**, 1891–1903 (2019)
17. Tanwar, D.V., Wazwaz, A.M.: Lie symmetries, optimal system and dynamics of exact solutions of (2+1)-dimensional KP-BBM equation. Phys. Scr. **95**, 065220 (2020)
18. Wang, D.S., Yin, S.J., Tian, Y., Liu, Y.F.: Integrability and bright soliton solutions to the coupled nonlinear Schrödinger equation with higher-order effects. Appl. Math. Comput. **229**, 296–309 (2014)
19. Wang, D.S., Wang, X.L.: Long-time asymptotics and the bright N-soliton solutions of the Kundu–Eckhaus equation via the Riemann–Hilbert approach. Nonlinear Anal. Real World Appl. **41**, 334–361 (2018)
20. Ma, W.X.: Riemann–Hilbert problems of a six-component fourth-order AKNS system and its soliton solutions. Comput. Appl. Math. **37**, 6359–6375 (2018)
21. Ma, W.X.: Riemann–Hilbert problems and soliton solutions of a multicomponent mKdV system and its reduction. Math. Methods Appl. Sci. **42**, 1099–1113 (2019)
22. Kang, Z.Z., Xia, T.C.: Construction of multi-soliton solutions of the N-coupled Hirota equations in an optical fiber. Chin. Phys. Lett. **36**, 110201 (2019)
23. Kang, Z.Z., Xia, T.C., Ma, W.X.: Riemann–Hilbert method for multi-soliton solutions of a fifth-order nonlinear Schrödinger equation. Anal. Math. Phys. **11**, 14 (2021)
24. Zhao, W.Z., Bai, Y.Q., Wu, K.: Generalized inhomogeneous Heisenberg ferromagnet model and generalized nonlinear Schrödinger equation. Phys. Lett. A **352**, 64–68 (2006)
25. Sun, H., Shan, W.R., Tian, B., Wang, M., Tan, Z.: Analytic studies on a generalized inhomogeneous higher-order nonlinear Schrödinger equation for the Heisenberg ferromagnetic spin chain. Commun. Nonlinear Sci. Numer. Simulat. **20**, 711–718 (2014)
26. Radha, R., Kumar, V.R.: Explode-decay solitons in the generalized inhomogeneous higher-order nonlinear Schrödinger equations. Z. Naturforsch. A **62**, 381–386 (2007)
27. Jia, H.X., Liu, Y.J., Wang, Y.N.: Rogue-wave interaction of a nonlinear Schrödinger model for the alpha helical protein. Z. Naturforsch. A **71**, 27–32 (2016)
28. Zuo, D.W., Gao, Y.T., Xue, L., Sun, Y.H., Feng, Y.J.: Rogue-wave interaction for the Heisenberg ferromagnetism system. Phys. Scr. **90**, 035201 (2015)
29. Wang, P., Qi, F.H., Yang, J.R.: Soliton solutions and conservation laws for an inhomogeneous fourth-order nonlinear Schrödinger equation. Comput. Math. Math. Phys. **58**, 1856–1864 (2018)
30. Yang, J.K.: Nonlinear Waves in Integrable and Nonintegrable Systems. SIAM, Philadelphia (2010)